InvoExNet: Explainable Involution Neural Network Framework for Biomedical Image Classification

Fahim Muntasir[1][0009−0007−2840−8605] Ayon Datta[2], M.F. Mridha[3][0000−0001−5738−1631], Nilanjan Dey[4][0000−0001−8437−498X], and Jungpil Shin[5][0000−0002−7476−2468]

[1] Department of Computer Science and Engineering, BRAC University, Dhaka, Bangladesh
muntasirfahim.niloy@gmail.com
[2] Department of Electrical and Electronic Engineering, Ahsanullah University of Science and Technology, Dhaka, Bangladesh
ayon2k15@gmail.com
[3] Department of Computer Science, American International University-Bangladesh, Dhaka, Bangladesh
firoz.mridha@aiub.edu
[4] Department of Computer Science and Engineering, Techno International New Town, Kolkata, India.
neelanjan.dey@gmail.com
[5] Department of Computer Science and Engineering, University of Aizu, Aizuwakamatsu, Japan
jpshin@u-aizu.ac.jp

Abstract. Involution Neural Networks have recently been introduced in place of famously used Convolution Neural Networks. INNs solve one of the core issues of CNN, inter-channel redundancy, resulting in fewer parameters. However, to fully shift from CNN models to INN models in biomedical image analysis, understanding the predicted outcome is very crucial. Our proposed 'InvoExNet' model combines an INN model with Local Interpretable Model-agnostic Explanations (LIME). Both INN and CNN models were tested against an imbalanced dataset of chest X-rays. In the same configuration, INN was found to use 78% fewer parameters while surpassing the CNN counterpart in terms of performance. This framework exhibits outstanding results and provides insights into the decision-making process of INN by utilizing LIME to offer clearer and more understandable predictions. A smaller and self-explanatory model can greatly aid healthcare professionals and early treatments.

Keywords: Involutional Neural Network · Explainable AI · Local Interpretable Model-agnostic Explanations (LIME)· Chest X-ray · Biomedical Imaging

1 Introduction

X-rays are electromagnetic radiations that pierce the human body, creating optical representations of its hidden architecture. Density-based object differentiation is based on the four basic densities observed on a radiograph: bone, soft tissues, fat and gas [6]. The penetrations of X-rays through these densities are contingent upon the level of exposure and the beam amplitude. There are two techniques for capturing X-ray images, posteroanterior (PA) and anteroposterior (AP). For posterior views, the X-ray beams impinge upon the patient from the posterior aspect, whereas for anterior views, the X-ray beams impinge against the patient's upper chest. Compared to AP views, PA images offer a more precise diagnosis of the lungs and heart [32]. The AP view is typically seen in bedridden, immobile patients utilizing portable X-ray equipment [17]. Visualizing the AP view, the heart and lungs look larger than their actual size, perhaps leading to a misdiagnosis of cardiomegaly in the patient. Physicians may also choose a lateral view to achieve a 3D perspective. The swift progress in computational power and the abundance of data have led to a remarkable growth in deep learning methods in recent years. Scientists are undertaking a global endeavour to develop technologies to aid radiologists in their diagnostic tasks. Several AI techniques are utilized to identify the optimal network for the domain of radiology and medical image processing [19].

The discipline of medical imaging has been drastically transformed by neural networks, particularly in the interpretation and processing of X-ray images. These complex algorithms can detect patterns and anomalies with precision and speed that exceed traditional approaches, hence assisting radiologists in detecting diseases with more efficacy [21]. Deep neural networks, applying extensive datasets, improve the early detection of diseases and the accuracy of therapy by identifying subtle characteristics in X-ray images, making them crucial in the medical field for reliable diagnosis [35]. Despite the considerable promise, neural networks in X-ray imaging have several problems. One remarkable concern is the interpretability of the models; it is sometimes obscure how these networks get their findings [28]. This might pose challenges in clinical environments where comprehending the reasoning behind a diagnosis is vital. Insufficient transparency can result in a dearth of confidence among healthcare practitioners, who may be reluctant to depend on a 'black-box' system [20]. Furthermore, neural networks are susceptible to overfitting, specifically when trained on restricted or unbalanced datasets, resulting in less dependable performance on a novel, unfamiliar material [34]. Disparities among institutions add complexity to the practical implementation of these models, which may lead to inconsistent diagnostic outcomes [31].

This paper focuses on implementing a deep learning framework with an Involution neural network(INN) and comparing it to the vastly used convolution neural network (CNN) in a similar setting. We will classify three diseases from X-ray images with the deep learning models. Our contribution is as follows:

- **Novel INN Architecture:** We propose an Involution neural network in classifying X-ray images. INNs, to the best of our knowledge, haven't been

used in a similar study. This novel architecture can be effective in biomedical image analysis applications.

- **Diversified Dataset:** We work with an imbalanced multiclass dataset of X-ray images. This dataset depicts a real-life scenario of a lack of medical image availability. It will also test the INN's ability to classify X-rays and overall label generalizing capability.
- **Comparative Analysis:** We compare several metrics from INN with existing algorithms such as CNN, AlexNet and a transformer model ResNet101. These have been most used in medical imaging since their introduction. Here, INN competes with these algorithms in exact hyper-parameter tuning.
- **Explaining INN Predictions:** In medical images, only a correct prediction is not enough to trust. We enhance confidence in our predictions by passing them via LIME Explainable AI and mapping out exact regions of the X-rays, INN have put importance on making that prediction. LIME also plots the probability distribution of all the regions, thus showing if INN focuses more on the background or the actual area of interest.

We believe these approaches won't make medical professionals obsolete in biomedical imaging, but rather should be used as a trustworthy and handy tool for easier inspection of X-ray images.

2 Related Work

Notably, it emphasises AI-powered medical imaging techniques that are prudent and conservative in their approach to COVID-19, including all imaging procedures from image acquisition to post-treatment monitoring. A range of image processing models, including CT scans, X-rays, mammographies, and pathological images, have been employed to integrate machine learning techniques into the domain of healthcare [14]. Recent developments in the field comprise the installation of a fuzzy classification and segmentation system for the identification of breast cancer using mammography images, the utilization of deep learning for the diagnosis of malaria by applying microscopic images of blood smears, and the utilization of unsupervised learning [25]. If the model has been trained and constructed with a high-quality deep learning model, a dataset of good quality can somewhat contribute to detecting the problem.

Multiple research in the field of radiology has revealed a remarkable degree of efficacy in executing artificial intelligence for the analysis of radiographic data. Therefore, a detailed analysis is required depending on deep learning to provide reliable and accurate predictions. Kallianos et al. [11] conducted a brief introduction on the new developments done on AI in the field of CXR interpretation. Nevertheless, the report is deficient in comprehensive details about the specific locations of different diseases in CXR, as its main priority is limited to consider the many architectural styles used by authors. Hence, the present study aims to rectify the found deficiencies.

In their study, Bar et al. [1] attained 89% accuracy for cardiomegaly on CXR images. Tariqul Islam et al. [8] in his study has utilized pre-trained ResNet-101 to identify cardiomegaly, and the accuracy of the same was found to be 92%. Tataru et al. [33] implemented pre-trained network ImageNet and ResNet101 and tried to detect 8 ordinary pathologies in the CXR images. Nevertheless, while the model accurately detected the presence of the disease, it failed to precisely ascertain the exact locations of the problems. Moreover, the multiple pathologies detection was tried to solve with the help of a preconfigured generic visual recognition model [29] [22]. However, again the model is inherently limited in its capability to recognize the existence of the disease, as it cannot precisely identify the specific spot of the disease. Specifically, Bouslama et al. [2] proposed a new U-Net-based CNN algorithm which obtained an accuracy between 93% and 94% on cardiomegaly detection and localization, something that had not been seen in previous attempts. For efficient identification of COVID-19 cases, Chassagnon et al. [24] presented a CNN-inspired 'nCOVnet' method trained on the ImageNet dataset and exploited VGG-16 for feature extraction. The model precisely categorized patients with a confidence level of 97.97% for Covid-19 positive patients and 98.68% for Covid-10 negative patients. Likewise, Ozturk et al. [23] sought to identify Covid-19 by developing the 'DarkCovidNet' architecture, which was influenced by the proven Darknet-19 model, a very efficient object identification model. The model under consideration has 27 convolution layers and 1125 images for training purposes, where 125 images are related to COVID-19, 500 images reflect Pneumonia, and 500 images with no identifiable cause. An accuracy of 98.08% was attained by the suggested model in classifying between COVID-19 and No-Findings. Khan et al. [13] developed an intricate 'CNN CoroNet' implemented on the Xception architecture, which had a notable accuracy rate of 89.6%; their study aimed to distinguish between three distinct forms of pneumonia, namely bacterial pneumonia, viral pneumonia, and Covid-19 pneumonia. Rajpurkar et al.[27] established an F1 score measure to assess Chexnet's pneumonia detection accuracy against four radiologists. The algorithm performed like an expert radiologist but better than an ordinary one. Jaiswal et al. [10] introduced a Mask-RCNN-inspired identification model with necessary training process adjustments and a unique post-processing stage that integrates bounding boxes from several models and eventually, their model performed better on CSR datasets showing pneumonia reasons. Hwang et al. [7] started employing deep learning to identify tuberculosis (TB) in 2016. KIT, NIH, and Shenzen datasets were applied to train and assess the pre-trained AlexNet model. The model has AUCs of 0.964, 0.88, and 0.93 for KIT, NIH, and Shenzen datasets. For its primary attempt, the model performed well, although the AUC varies between datasets suggesting AI overfitting. Lakhani and Sundaram expanded AI-based TB detection [16]. Cross-dataset validity was achieved using trained and untrained GoogleNet and AlexNet models on four datasets. Untrained models had AUCs of 0.90 and 0.88, whereas pre-trained models had 0.98 and 0.97.

3 Methodology

Fig. 1 depicts the workflow of the InvoExNet framework. The X-ray database was formed by gathering X-rays of three different types of diseases and regular X-rays. The images were then cropped and normalized for a streamlined input to the neural network model. The class imbalance can be seen in table 1. The data was fed to the Involution Neural Network in 16 images of 250*250*3 dimension per batch format. The final dense layer returned the probabilities of each class. ArgMax converted them into predictions. Lastly, the projections were passed to the LIME image explainer. This ensured that the INN model looked at the affected superpixel or regions.

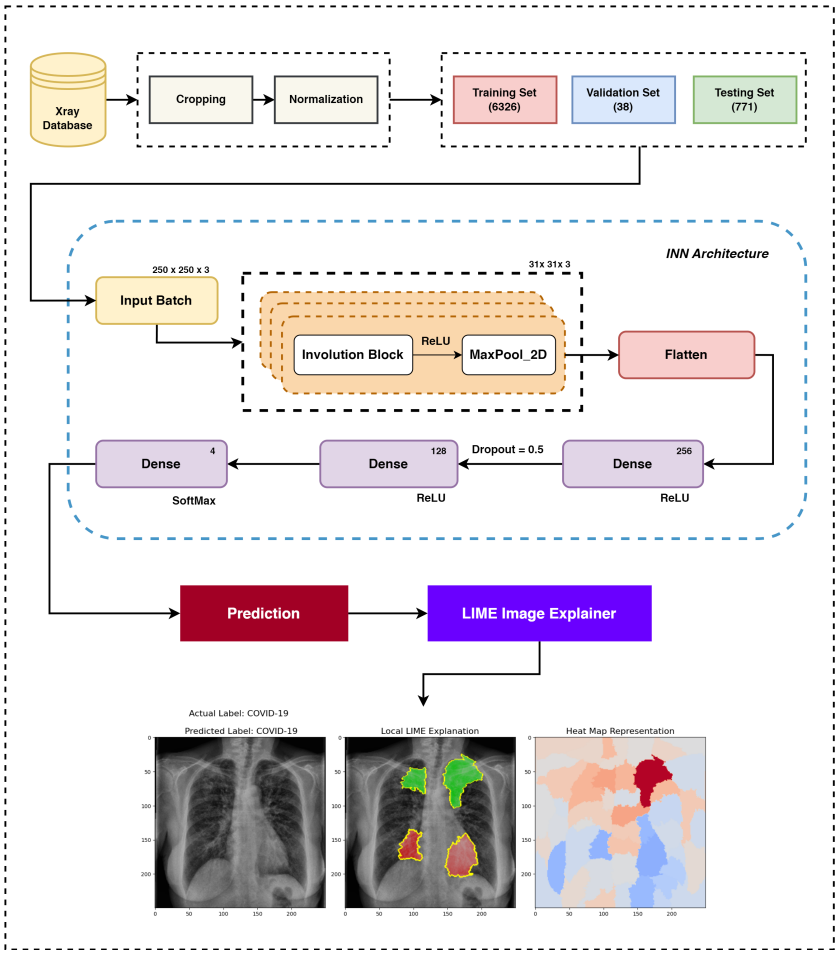

Fig. 1: Workflow diagram of InvoExNet framework

3.1 Dataset

The dataset used for this research was collected from several sources [12] [26] [3]. A total of 7,135 chest X-ray scans from four separate classes. The photos were separated into three sets: training, testing, and validation. Each category comprises sub-folders with photos categorized into four conditions: tuberculosis (TB), COVID-19, pneumonia, and normal. The dataset, however, suffers greatly from class imbalance. All the images were cropped to the same size and normalized while taken as input by the models.

Table 1: Image count in training, testing and validation set

Class	**Training**	**Testing**	**Validation**
Covid-19	460	106	10
Normal	1341	234	8
Pneumonia	3875	390	8
Tuberculosis	650	41	12

3.2 Convolution Neural Network

Rather than using conventional machine learning, we chose to apply deep learning for this multiclass image classification task. Multiple models were examined in the identical configuration. The architectural design of the INN model is elaborated further in another part.

- **Alexnet:** The convolutional neural network architecture known as AlexNet has a profound impact on deep learning and computer vision [15]. The architecture includes 8 layers and utilizes mechanisms such as ReLU activation, random cropping, LRN and colour jittering. Alexnet proved the greater effectiveness of Convolutional Neural Networks (CNNs) compared to traditional image classification methods.
- **ResNet101 V2:** ResNet101 V2 is a well-renowned deep learning architecture, popular for its exceptional performance in image classification tasks [4]. The residual blocks of the system design integrate identity mappings and use a bottleneck architecture to minimize computing expanses. Moreover, preactivation residual units are executed to improve the training process.
- **ConvoNet:** This is the base CNN model. It was built from scratch with three CNN layers followed by max-pooling and relu activation functions. These feature vectors were then flattened and passed via several dense layers to the final output layer. This model was built as a head-to-head comparison to the INN model.

3.3 Involution Neural Network

Involution was introduced as the opposite of convolution in [18]. Instead of using a fixed set of convolutional filters, involution uses a more flexible operation where the kernel is dynamically generated based on the input features. This dynamic kernel adapts to different spatial positions in the input, allowing the network to capture more complex patterns with fewer parameters. This greatly reduces the complexity of the total model. While filters in CNNs are channel-specific and spatial agnostic, this often creates inter-channel redundancy [9]. Involution aggregates context in a larger spatial arrangement, making it easier to simulate long-range interactions. It can also distribute weights to prioritize the most useful visual features in the domain. Opposite to CNN, INNs are Location-specific and channel-agnostic. The involution operation is designed to adapt to different spatial locations within the input image (location-specific) while treating all channels equally without differentiating between them (channel-agnostic). This can be very useful in medical image analysis.

3.4 Evaluation Metrics

We compared the parameter counts of the models to understand their efficiency. A small model will have reduced computational cost, lower memory consumption and less prone to over-fit. On the other hand, to understand the multi-label classification performance, we opted for several metrics. Accuracy, precision, recall and F1 scores were the evaluators for the trained models [5]. A normalized confusion matrix was also plotted to understand the predictions. Only relying on accuracy can sometimes lead to misleading higher performance, while actual prediction is wrong. A confusion matrix solves this easily by plotting the percentage of correct and incorrect predictions.

3.5 LIME Explainable AI

LIME stands for Local Interpretable Model-Agnostic Explanations. This leverages quick-shift segmentation to create superpixels of the actual image [30]. It determines the tiny features that contribute to the highest likelihood of a class result for a given observation. The purpose of this study is to evaluate the usefulness of LIME explanations and how they affect healthcare professionals' faith in black-box classification techniques. LIME consists of several processes, including picking an event, altering data, predicting results, and developing a transparent model.

4 Result Analysis

we applied well-known and often-used measures for evaluation. Various metrics provided a clearer interpretation of the models without delving into the complexities of concepts such as true positive, false negative and so on. As this is a

multi-class classification task and we assigned the same weight to each class, we used the 'weighted average' methodology. Table 2 shows that AlexNet achieves 85.15% accuracy with a moderate number of parameters (29.98 million). Its performance is fairly balanced across all metrics, but it does not excel in any particular one. ResNet101 V2 shows the highest accuracy (88.72%) and F1 Score (89.75), indicating a strong overall performance. However, this comes at the cost of a large number of parameters (43.74 million), which can make the model computationally expensive. ConvoNet has the lowest performance in terms of accuracy (77.82%) and F1 Score (74.39), but it also has a high parameter count (55.28 million). This suggests that despite its complexity, it is not as effective as the other models. InvoExNet demonstrates strong performance with an accuracy of 84.31%, precision of 84.75%, recall of 84.31%, and an F1 Score of 83.72%. Remarkably, it achieves these results with only 0.7 million parameters, significantly fewer than all other models.

Table 2: Performance (Weighted Average) comparison of all models.

Architecture	**Accuracy**	**Precision**	**Recall**	**F1 Score**	**Parameter In Million**
AlexNet	85.15	83.20	82.15	82.65	29.98
ResNet101 V2	88.72	90.83	88.72	89.75	43.74
ConvoNet	77.82	82.13	77.82	74.39	55.28
InvoExNet	**84.31**	**84.75**	**84.31**	**83.72**	**0.7**

InvoExNet outperforms the other models when considering the trade-off between performance and computational efficiency. While ResNet101 V2 has slightly higher accuracy and F1 Score, it requires 42-78% more parameters than InvoExNet. This makes InvoExNet much more efficient in terms of computational resources, achieving comparable performance with far fewer parameters. This efficiency is crucial for applications requiring quick inference times or deployment on devices with limited processing power. Therefore, InvoExNet offers a superior balance of performance and parameter efficiency, outperforming the other models in scenarios where resource constraints are a consideration.

In Fig. 2, the prediction performance of both ConvoNet and InvoExNet are compared using confusion matrices to provide normalized predictions across four classes: normal, COVID-19, pneumonia, and tuberculosis. We see that both the CNN and INN models performed closely. However, CNN failed to normalize its output across all the classes. Moreover, the CNN model hallucinated largely between normal and pneumonia classes. INN model, on the contrary, showed much lesser hallucination. Also, CNN mostly caused type-II errors, but the ones from INN were mostly type-I. It is truly astounding that INN outperformed CNN while using 78% fewer parameters.

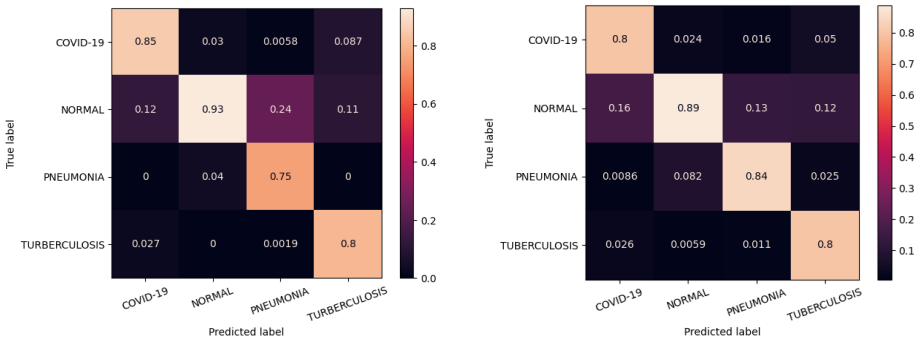

(a) ConvoNet (b) InvoExNet

Fig. 2: Normalized (pred) confusion matrix of predictions

Fig. 4 and 3 depict the training and validation curves of the two different neural network models. InvoExNet seems to own a more optimal equilibrium between the procedures of learning and generalization. Notwithstanding minor variations in validation accuracy, the model effectively handles the validation data, without any overfitting. On the other hand, the ConvoNet model exhibits hallmark indications of overfitting. The training accuracy is virtually flawless, and the training loss is negligible. However, the validation performance is poor, characterized by significant loss and low accuracy, suggesting a reduced capacity of the model to generalize. In comparison to ConvoNet, which exhibits overfitting in the training data and faces challenges with validation data, InvoExNet exhibits superior generalization abilities.

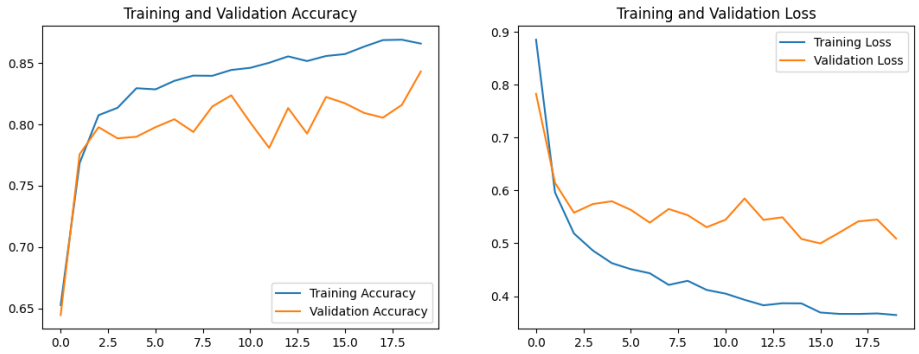

Fig. 3: Training and validation curves of InvoExNet

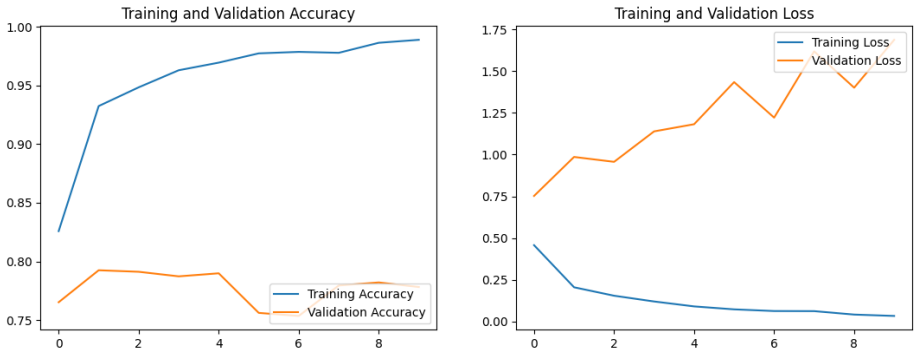

Fig. 4: Training and validation curves of ConvoNet

5 Lime Explanataion

Noticing from Fig. 5, 6, 7 and 8, the LIME explanation separates images by colour, brightness, hue and saturation. LIME identifies how the INN model segments these. LIME samples are shown in the above-mentioned figure, each has 3 consoles. The first console represents the forecast, the second the pros-cons sections found by LIME, and the third a heatmap of LIME's explanation. LIME starts by isolating the images into superpixels. These continuous image patches have similar hues and brightness. Green shade represents pros and red represents drawbacks on the second console. The red tones on the third console suggest the INN algorithm prioritized these locations for categorization. Bluish spots are lighter.

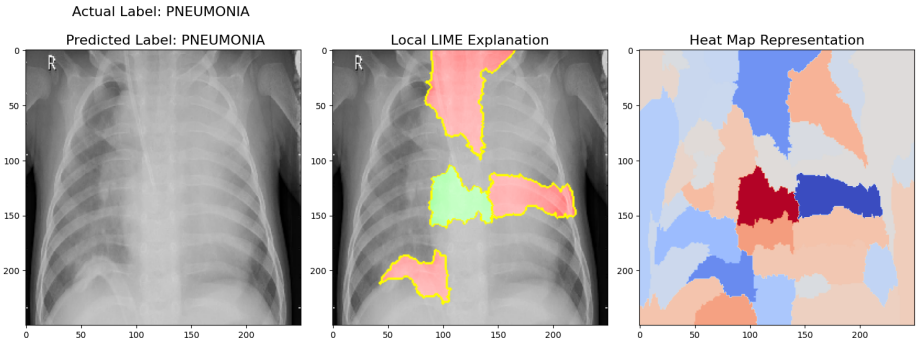

Fig. 5: LIME Explanation on pneumonia sample

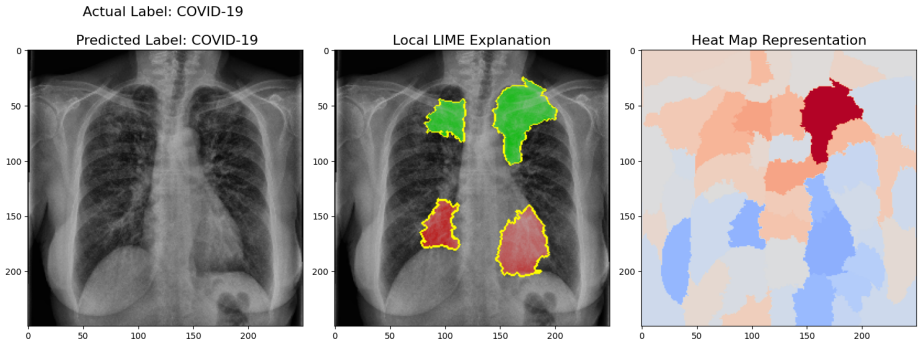

Fig. 6: LIME Explanation on Covid-19 sample

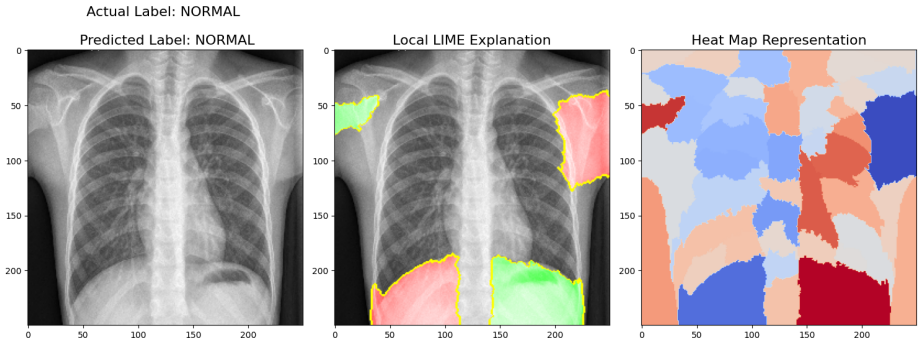

Fig. 7: LIME Explanation on normal sample

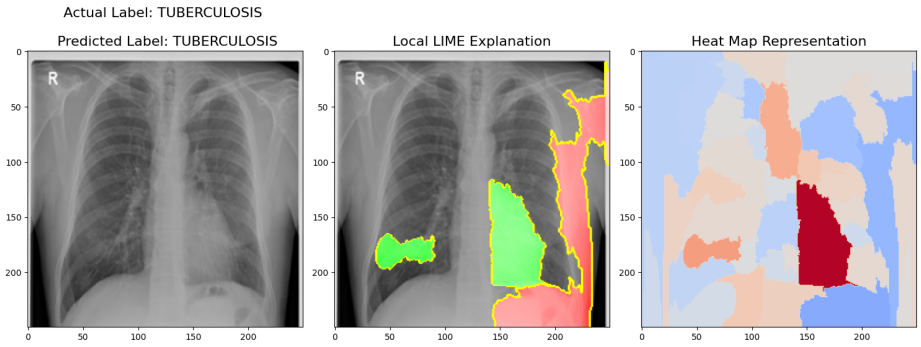

Fig. 8: LIME Explanation on tuberculosis sample

6 Conclusion

The InvoExNet model is proposed to address the transparency issues of neural networks in identifying multi-class diseases from CXR images. Our deployment of an Explainable Involutional Neural Network model for classification has shown superior performance in comparison to concurrent CNN architectures and transformer models using pre-trained weights. This innovative approach incorporates INN with LIME method to locate the unpredictability in image quality. The complementary nature of INN and LIME enables the development of image classification models that are both highly efficient and easily understandable. INN, here, improves the model's capacity to comprehend subtle features in images, while LIME guarantees that these features can be understood well, hence increasing the clarity and reliability of the model's predictions. The outcomes of the models might help researchers and practitioners integrate XAI to evaluate patients with COVID-19, Tuberculosis, and Pneumonia using Chest X-ray images.

References

1. Bar, Y., Diamant, I., Wolf, L., Greenspan, H.: Deep learning with non-medical training used for chest pathology identification. In: Medical Imaging 2015: Computer-Aided Diagnosis. vol. 9414, pp. 215–221. SPIE (2015)
2. Bouslama, A., Laaziz, Y., Tali, A.: Diagnosis and precise localization of cardiomegaly disease using u-net. Informatics in Medicine Unlocked **19**, 100306 (2020)
3. Cohen, J.P., Morrison, P., Dao, L.: Covid-19 image data collection. arXiv 2003.11597 (2020), https://github.com/ieee8023/covid-chestxray-dataset
4. Gao, R., Wang, R., Feng, L., Li, Q., Wu, H.: Dual-branch, efficient, channel attention-based crop disease identification. Computers and Electronics in Agriculture **190**, 106410 (2021)
5. Grandini, M., Bagli, E., Visani, G.: Metrics for multi-class classification: an overview. arXiv preprint arXiv:2008.05756 (2020)
6. Hu, M., Lin, H., Fan, Z., Gao, W., Yang, L., Liu, C., Song, Q.: Learning to recognize chest-xray images faster and more efficiently based on multi-kernel depthwise convolution. IEEE Access **8**, 37265–37274 (2020)
7. Hwang, S., Kim, H.E., Jeong, J., Kim, H.J.: A novel approach for tuberculosis screening based on deep convolutional neural networks. In: Medical imaging 2016: computer-aided diagnosis. vol. 9785, pp. 750–757. SPIE (2016)
8. Islam, M.T., Aowal, M.A., Minhaz, A.T., Ashraf, K.: Abnormality detection and localization in chest x-rays using deep convolutional neural networks. arXiv preprint arXiv:1705.09850 (2017)
9. Jaderberg, M., Vedaldi, A., Zisserman, A.: Speeding up convolutional neural networks with low rank expansions. arXiv preprint arXiv:1405.3866 (2014)
10. Jaiswal, A.K., Tiwari, P., Kumar, S., Gupta, D., Khanna, A., Rodrigues, J.J.: Identifying pneumonia in chest x-rays: A deep learning approach. Measurement **145**, 511–518 (2019)
11. Kallianos, K., Mongan, J., Antani, S., Henry, T., Taylor, A., Abuya, J., Kohli, M.: How far have we come? artificial intelligence for chest radiograph interpretation. Clinical radiology **74**(5), 338–345 (2019)

12. Kermany, D.S., Goldbaum, M., Cai, W., Valentim, C.C., Liang, H., Baxter, S.L., McKeown, A., Yang, G., Wu, X., Yan, F., et al.: Identifying medical diagnoses and treatable diseases by image-based deep learning. cell **172**(5), 1122–1131 (2018)
13. Khan, A.I., Shah, J.L., Bhat, M.M.: Coronet: A deep neural network for detection and diagnosis of covid-19 from chest x-ray images. Computer methods and programs in biomedicine **196**, 105581 (2020)
14. Kretz, T., Müller, K.R., Schaeffter, T., Elster, C.: Mammography image quality assurance using deep learning. IEEE Transactions on Biomedical Engineering **67**(12), 3317–3326 (2020)
15. Krizhevsky, A., Sutskever, I., Hinton, G.E.: Imagenet classification with deep convolutional neural networks. Advances in neural information processing systems **25** (2012)
16. Lakhani, P., Sundaram, B.: Deep learning at chest radiography: automated classification of pulmonary tuberculosis by using convolutional neural networks. Radiology **284**(2), 574–582 (2017)
17. Laserson, J., Lantsman, C.D., Cohen-Sfady, M., Tamir, I., Goz, E., Brestel, C., Bar, S., Atar, M., Elnekave, E.: Textray: Mining clinical reports to gain a broad understanding of chest x-rays. In: Medical Image Computing and Computer Assisted Intervention–MICCAI 2018: 21st International Conference, Granada, Spain, September 16-20, 2018, Proceedings, Part II 11. pp. 553–561. Springer (2018)
18. Li, D., Hu, J., Wang, C., Li, X., She, Q., Zhu, L., Zhang, T., Chen, Q.: Involution: Inverting the inherence of convolution for visual recognition. In: Proceedings of the IEEE/CVF conference on computer vision and pattern recognition. pp. 12321–12330 (2021)
19. Liew, Y.M., McLaughlin, R., Chan, B., Aziz, Y.A., Chee, K., Ung, N., Tan, L., Lai, K., Ng, S., Lim, E.: Motion corrected lv quantification based on 3d modelling for improved functional assessment in cardiac mri. Physics in Medicine & Biology **60**(7), 2715 (2015)
20. López-Cabrera, J.D., Orozco-Morales, R., Portal-Diaz, J.A., Lovelle-Enríquez, O., Pérez-Díaz, M.: Current limitations to identify covid-19 using artificial intelligence with chest x-ray imaging. Health and Technology **11**(2), 411–424 (2021)
21. Mohammed, M.A., Abdulkareem, K.H., Garcia-Zapirain, B., Mostafa, S.A., Maashi, M.S., Al-Waisy, A.S., Subhi, M.A., Mutlag, A.A., Le, D.N.: A comprehensive investigation of machine learning feature extraction and classificationmethods for automated diagnosis of covid-19 based on x-ray images. Computers, Materials & Continua **66**(3) (2021)
22. Nizar, M.H.A., Khalil, A., Chan, C.K., Utama, N.P., Lai, K.W.: Pilot study on machine learning for aortic valve detection in echocardiography images. Journal of Medical Imaging and Health Informatics **9**(1), 9–14 (2019)
23. Ozturk, T., Talo, M., Yildirim, E.A., Baloglu, U.B., Yildirim, O., Acharya, U.R.: Automated detection of covid-19 cases using deep neural networks with x-ray images. Computers in biology and medicine **121**, 103792 (2020)
24. Panwar, H., Gupta, P., Siddiqui, M.K., Morales-Menendez, R., Singh, V.: Application of deep learning for fast detection of covid-19 in x-rays using ncovnet. Chaos, Solitons & Fractals **138**, 109944 (2020)
25. Pattanaik, P.A., Mittal, M., Khan, M.Z.: Unsupervised deep learning cad scheme for the detection of malaria in blood smear microscopic images. IEEE Access **8**, 94936–94946 (2020)
26. Rahman, T., Khandakar, A., Kadir, M.A., Islam, K.R., Islam, K.F., Mazhar, R., Hamid, T., Islam, M.T., Kashem, S., Mahbub, Z.B., et al.: Reliable tuberculosis

detection using chest x-ray with deep learning, segmentation and visualization. Ieee Access **8**, 191586–191601 (2020)
27. Rajpurkar, P., Irvin, J., Zhu, K., Yang, B., Mehta, H., Duan, T., Ding, D., Bagul, A., Langlotz, C., Shpanskaya, K., et al.: Chexnet: Radiologist-level pneumonia detection on chest x-rays with deep learning. arXiv preprint arXiv:1711.05225 (2017)
28. Rasheed, J., Hameed, A.A., Djeddi, C., Jamil, A., Al-Turjman, F.: A machine learning-based framework for diagnosis of covid-19 from chest x-ray images. Interdisciplinary Sciences: Computational Life Sciences **13**, 103–117 (2021)
29. Ren, N.n., Ma, A.r., Han, L.b., Sun, Y., Shao, Y., Qiu, J.f.: Automatic radiographic position recognition from image frequency and intensity. Journal of healthcare engineering **2017**(1), 2727686 (2017)
30. Ribeiro, M.T., Singh, S., Guestrin, C.: " why should i trust you?" explaining the predictions of any classifier. In: Proceedings of the 22nd ACM SIGKDD international conference on knowledge discovery and data mining. pp. 1135–1144 (2016)
31. Santos, C.F.G.D., Papa, J.P.: Avoiding overfitting: A survey on regularization methods for convolutional neural networks. ACM Computing Surveys (CSUR) **54**(10s), 1–25 (2022)
32. Santosh, K., Antani, S.: Automated chest x-ray screening: Can lung region symmetry help detect pulmonary abnormalities? IEEE transactions on medical imaging **37**(5), 1168–1177 (2017)
33. Tataru, C., Yi, D., Shenoyas, A., Ma, A.: Deep learning for abnormality detection in chest x-ray images. In: IEEE conference on deep learning. IEEE Adelaide (2017)
34. Ying, X.: An overview of overfitting and its solutions. In: Journal of physics: Conference series. vol. 1168, p. 022022. IOP Publishing (2019)
35. Zhao, X., Luo, Y., Liu, J., Liu, W., Rosso, K.M., Guo, X., Geng, T., Li, A., Zhang, X.: Machine learning automated analysis of enormous synchrotron x-ray diffraction datasets. The Journal of Physical Chemistry C **127**(30), 14830–14838 (2023)